J. Geophys. Eng. **4** (2007) 171–183 doi:10.1088/1742-2132/4/2/006

Rock classification based on resistivity patterns in electrical borehole wall images

Margarete Linek[1], **Matthias Jungmann**[2], **Thomas Berlage**[2,3], **Renate Pechnig**[1] **and Christoph Clauser**[1]

[1] Applied Geophysics, RWTH Aachen University, Lochnerstr. 4-20, 52056 Aachen, Germany
[2] Fraunhofer Institute for Applied Information Technology (FIT), Schloss Birlinghoven, 53754 St. Augustin, Germany
[3] Informatics *V*, RWTH Aachen University, Ahornstr. 55, 52056 Aachen, Germany

E-mail: m.linek@geophysik.rwth-aachen.de

Received 15 August 2006
Accepted for publication 14 February 2007
Published 23 March 2007
Online at stacks.iop.org/JGE/4/171

Abstract
Electrical borehole wall images represent grey-level-coded micro-resistivity measurements at the borehole wall. Different scientific methods have been implemented to transform image data into quantitative log curves. We introduce a pattern recognition technique applying texture analysis, which uses second-order statistics based on studying the occurrence of pixel pairs. We calculate so-called Haralick texture features such as contrast, energy, entropy and homogeneity. The supervised classification method is used for assigning characteristic texture features to different rock classes and assessing the discriminative power of these image features. We use classifiers obtained from training intervals to characterize the entire image data set recovered in ODP hole 1203A. This yields a synthetic lithology profile based on computed texture data. We show that Haralick features accurately classify 89.9% of the training intervals. We obtained misclassification for vesicular basaltic rocks. Hence, further image analysis tools are used to improve the classification reliability. We decompose the 2D image signal by the application of wavelet transformation in order to enhance image objects horizontally, diagonally and vertically. The resulting filtered images are used for further texture analysis. This combined classification based on Haralick features and wavelet transformation improved our classification up to a level of 98%. The application of wavelet transformation increases the consistency between standard logging profiles and texture-derived lithology. Texture analysis of borehole wall images offers the potential to facilitate objective analysis of multiple boreholes with the same lithology.

Keywords: pattern recognition, borehole geophysics, texture analysis, electrical borehole wall images, classification

1. Introduction

The Ocean Drilling Program (ODP) (1984–2003) and the follow-up Integrated Ocean Drilling Program (IODP) are long-term international scientific projects exploring the history of ocean basins and the oceanic crust by drilling. The main information comes from core recovered from the drilled holes (e.g. Benaouda *et al* (1999)). Since core recovery is often only partial, downhole measurements play a crucial role in providing data where core sections cannot be obtained. Lithology reconstruction using logging data is based on the concept of electrofacies (Serra 1986), which has been successfully applied to crystalline rocks (Bartetzko *et al* 2002, Pechnig *et al* 1997). This method translates measurements of physical properties from logs into lithological terms. A set of log responses is assigned to lithological facies within

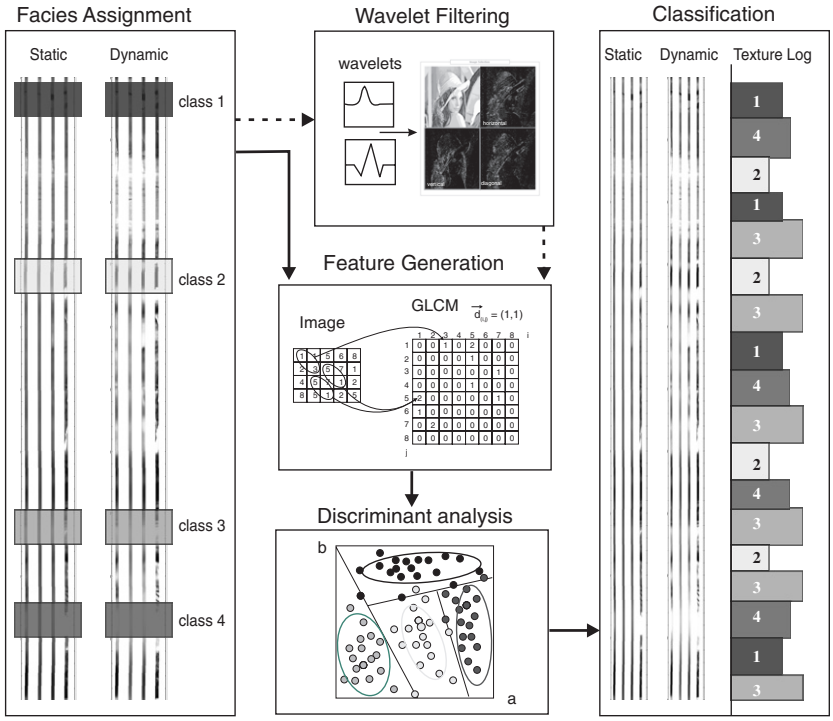

Figure 1. Our image processing workflow: (1) assignment of rock facies, (2) optional wavelet filtering, (3) feature generation and extraction based on Haralick texture features, (4) determination of a classification function based on discriminant analysis and finally, (5) classification of entire FMS images.

training intervals and reduced to a classifier function in order to characterize rock at depth intervals outside the training intervals (Bartetzko *et al* 2002, Benaouda *et al* 1999).

Within the ODP, the Formation MicroScanner (FMS) image logging tool is routinely deployed, representing resistivity measurements at the borehole wall in colour coding. Mostly, the image evaluation is based on visual inspection. The integration of FMS images and core data has provided detailed stratigraphic information on carbonate platforms (Cooper *et al* 1995), volcaniclastic sequences (Pezard *et al* 1992), as well as for facies reconstruction of extrusive sequences (Bartetzko *et al* 2003) and basement lithology (Barr *et al* 2002). Different approaches have been made to quantify information from borehole wall images in a similar way to the electrofacies log. Tyagi and Bhaduri (2002) translated the resistivity measured by individual buttons into porosity using Archie's law and analysed the resulting porosity histogram for each depth point with respect to porosity heterogeneities. Delhomme (1992) applied mathematical morphology for image segmentation to quantify resistivity heterogeneity. Textural segmentation based on Law's energy was implemented by Luthi (1994). In this case, the image is filtered by assigned texture masks and the resulting variance between mask and image is studied to classify bedding units. Machecler and Nadal (2004) proposed an image processing workflow depending on textural characteristics and type of segmentation (contour enhancement or texture edge detection) to extract the oriented textured feature boundaries without prior classification. Ye *et al* (1998) and Knecht *et al* (2003) combined first-order parameters derived from histogram and second-order statistics (study of pixel pairs), such as auto-covariance to analyse sedimentary sequences. Geostatistical analysis, another second-order statistic, was applied by Tilke *et al* (2006) to derive porosity from borehole wall images.

In this paper, we also present a method based on the study of pixel pairs. Our study is focused on the grey-level distribution of FMS images as was successfully performed for photographic core images by Harris *et al* (1993). We derive texture features from FMS images and assign texture facies to each rock class. Based on supervised statistical classification techniques, we apply the classifiers obtained from training intervals to the entire borehole.

The paper is organized as follows. The main part describes our approach used to transform FMS image data into quantitative log curves applying Haralick texture features. The proposed image processing workflow is shown in figure 1. The second part of the paper presents a case study from the ODP. We apply this technique to data from ODP hole 1203A drilled during Leg 197 in the northwest Pacific Ocean in which volcaniclastic sediments, pillow and massive basalts were recovered (Shipboard Scientific Party 2002).

2. FMS data acquisition and image processing

The Formation MicroScanner (FMS) was developed for micro-resistivity measurements and maps the electrical conductivity at the borehole wall. The tool is equipped with four perpendicularly exposed arms which are opened downhole and

Table 1. Common texture features computed from grey-level co-occurrence matrix $C(i, j)$ (Van de Wouver *et al* 1999).

Haralick feature	Formula
Contrast	$F_1 = \sum_{(i;j=0)}^{n} (i-j)^2 * C(i,j)$
Energy	$F_2 = \sum_{(i;j=0)}^{n} C^2(i,j)$
Entropy	$F_3 = -\sum_{(i;j=0)}^{n} C(i,j) * \log C(i,j)$
Local homogeneity	$F_4 = \sum_{(i;j=0)}^{n} \frac{1}{1+(i-j)^2} * C(i,j)$
Maximum probability	$F_5 = \max C(i,j)$
Cluster shade	$F_6 = \sum_{(i;j=0)}^{n} (i - M_x + j - M_y)^3 * C(i,j)$
Cluster prominence	$F_7 = \sum_{(i;j=0)}^{n} (i - M_x + j - M_y)^4 * C(i,j)$
Information measure of correlation	$F_8 = \frac{(C_3 - H_{xy})}{\max\{H_x, H_y\}}$
where	
$M_x = \sum_{(i;j=0)}^{n} i * C(i,j)$	$M_y = \sum_{(i;j=0)}^{n} j * C(i,j)$
$S_x(i) = \sum_{(j=0)}^{n} C(i,j)$	$S_y(j) = \sum_{(i=0)}^{n} C(i,j)$
$H_{xy} = -\sum_{(i,j=0)}^{n} C(i,j) \log(S_x(i) S_y(j))$	
$H_x = -\sum_{(i=0}^{n} S_x(i) * \log S_x(i)$	$H_y = -\sum_{(j=0}^{n} S_y(j) * \log S_y(j)$

force each pad against the borehole during upward logging. Each pad comprises an array of 16 button electrodes (Lovell *et al* 1998). A single pass of the tool measures about 30% of a 25.4 cm diameter borehole as typically drilled in ODP (Pezard *et al* 1992). During logging, a current flows from each electrode to a single return electrode located at the tool top. Due to the sensor geometry, the tool signal has a shallow penetration depth of a few centimetres beyond the borehole wall. The multiple button electrodes are held at a constant potential relative to the return electrode. A variable current is supplied to each electrode to maintain the constant potential. This current is related to the electrical conductivity of the borehole wall. Since electrical images are based on a two-electrode measurement, they do not represent true formation resistivity (Pezard *et al* 1992, Lovell *et al* 1998) but, rather, relative changes in electrical conductivity (Cheung 1999). The sampling rate of the FMS tool is about 2.5 mm corresponding to a vertical resolution of about 5 mm (Goldberg 1997). Arm extension is used to measure the borehole diameter between pad pairs 1–3 and 2–4, respectively. The maximum extension of the caliper arms is 38.1 cm (15.0 inch). If the borehole exceeds this diameter (washouts), the pad contact will be inconsistent and the FMS image will be de-focused and blurred (Barr *et al* 2002). Consequently, image interpretation of corresponding pads is inhibited.

Image processing converts the current intensities measured by each electrode into images: the current intensity is translated into a variable intensity of colour or grey-level images through a series of processing steps which include corrections for variations in focusing current and tool speed. The resulting image is then normalized statically so that each grey level corresponds to a distinct current intensity for the entire image. This results in a large-scale visualization of data and permits us to compare data along the entire log. In contrast, important fine details are visualized by dynamic normalization which enhances local details through histogram equalization within a sliding window (Lovell *et al* 1998). In our study, light and dark grey levels represent resistive parts and conductive borehole wall features, respectively.

3. Texture analysis

We apply pattern recognition techniques on borehole wall images in order to progress from qualitative and subjective to quantitative and objective image interpretation. Pattern recognition aims to classify data based on statistical information extracted from patterns (Duda *et al* 2001). We focus on texture-based analysis. Image texture is defined as a function of the spatial variation in grey level intensities (Tuceryan and Jain 1998). It plays an important role in many image processing tasks, ranging from medical imaging to remote sensing (Van de Wouver *et al* 1999). First-order texture parameters are based on the statistics of single-pixel grey levels. Second-order parameters reflect the statistics of grey level pairs (Van De Wouver 1998). We apply texture analysis to FMS borehole wall images using second-order parameters in order to classify rocks based on their resistivity contrast. The first step of texture analysis is feature extraction, which reduces the image to a set of descriptive features. The second step classifies image parts based on the features computed from the pixel pairs. The main analysis tool for texture feature extraction is the so-called grey level co-occurrence matrix (C), which counts the presence of grey level pairs (i, j) for a given displacement vector $\vec{d}$ (see figure 2) (Tuceryan and Jain 1998, Van De Wouver 1998). Common co-occurrence parameters, known as so-called Haralick texture features (Jain *et al* 2000), are listed in table 1. We used a rotation-invariant parameter configuration, which means we applied four different displacement vectors as displayed in figure 2 to calculate the matrix $C(i, j)$. Then, we determined the texture feature from each matrix, and finally averaged the directional results for each depth point. Figure 3 represents a set of Haralick log curves computed from a static FMS image.

In addition, we considered the distribution of the texture features up to the fourth statistical moments such as expectation (first moment), variance (second moment), skewness (third moment) and kurtosity (fourth moment). These four moments of each texture feature are derived from data within a 50 cm long sliding window. These

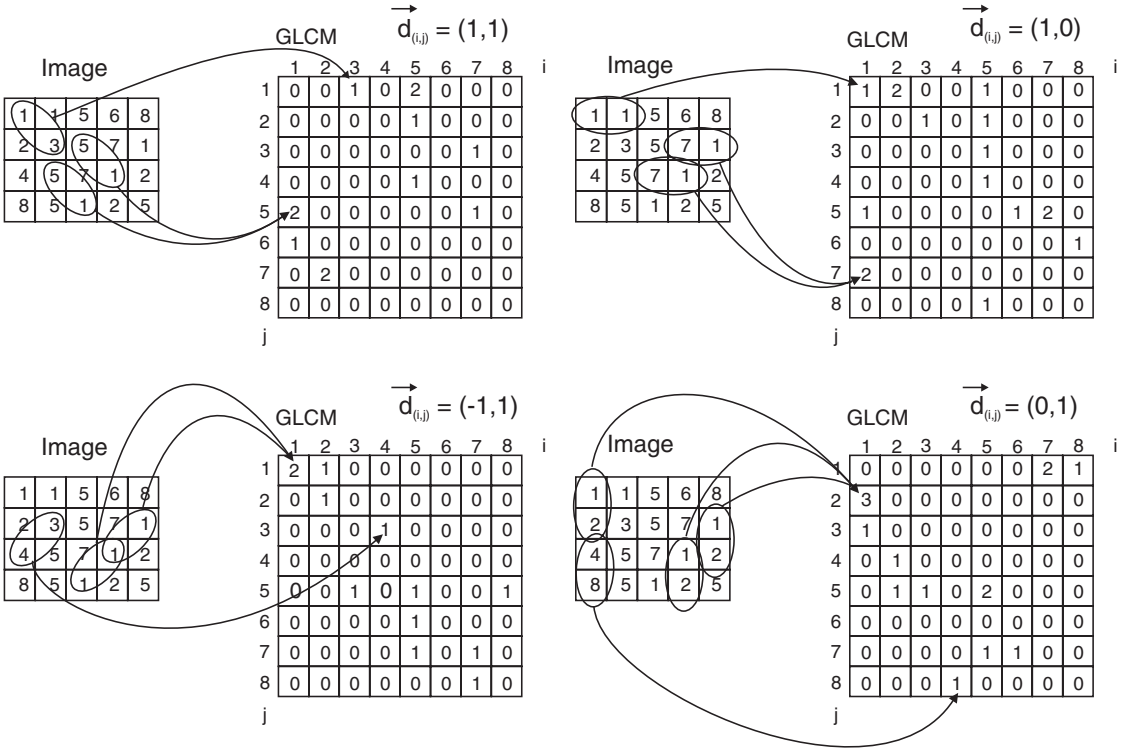

Figure 2. An image is an array of grey levels. Determination of the grey level co-occurrence matrix (GLCM) C: the entry (i, j) is the number of occurrences of the grey level pair i and j that are a distance d apart (Tuceryan and Jain 1998, Van De Wouver 1998). The GLCM was computed for four distinctive directions: along two diagonals, the vertical, and the horizontal direction.

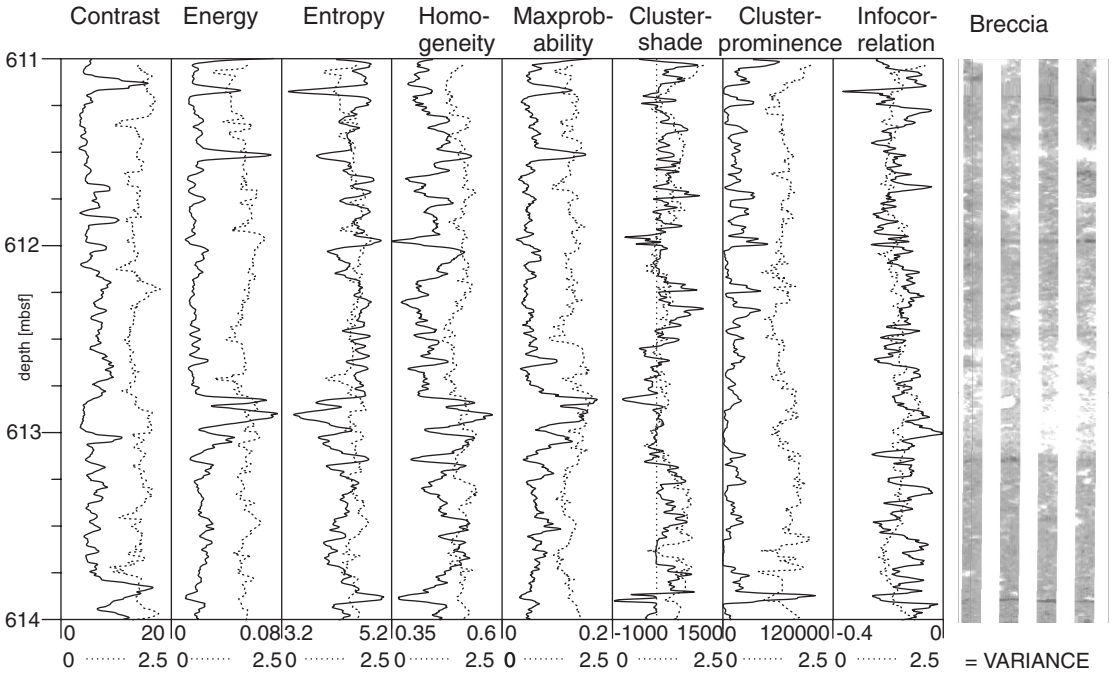

Figure 3. FMS image data have been transferred into log curves. Statistical moments (e.g. variances) were also computed for classification.

statistical moments of the Haralick texture features are used for classification.

In our study, the FMS images were processed based on a 64-grey-level scale. Hence, the matrix C has a dimension of 64 × 64. In order to determine this matrix, we use a sliding window of 16 × 16 pixels, which represents the entire pad width (16 electrodes). Parameters derived from each window are depth-related to the centre of each window. We use both the dynamic and the static normalization in our study. These differently processed images are simultaneously included in

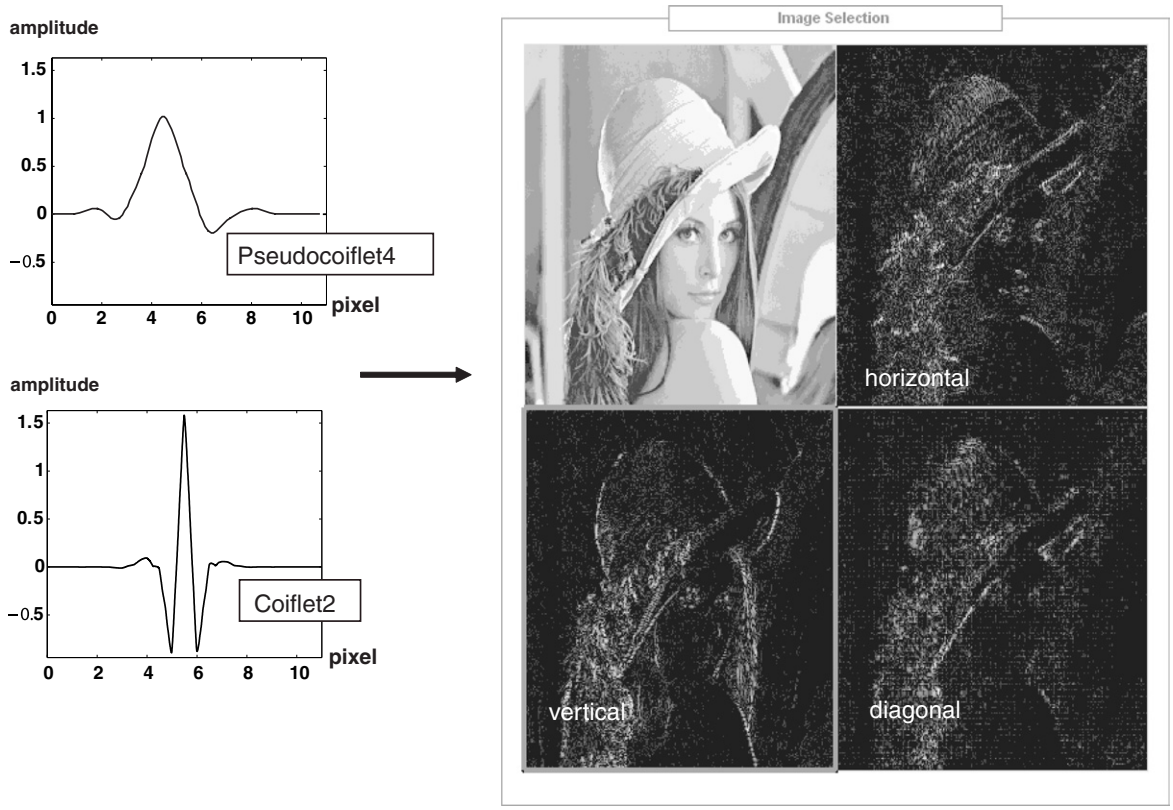

Figure 4. Multiscale representation of depth $d = 1$ of the Lena image (test image of the Signal and Image Processing Institute of the University of Southern California (USA)). Wavelets used for single level image decomposition: the vertical detail image obtained by Coiflet 2 as well as the diagonal detail image derived from Pseudocoiflet 4.

the analysis. We tested the improvement of classification by using either dynamically or statically processed images in comparison to considering both image types simultaneously. We found that increasing the feature space by considering both processed image types at once had a considerable influence on the classification results. Using just statically processed images did not allow us to distinguish the assigned igneous rock classes satisfactorily. Including the feature space of dynamically processed images in the analysis, however, significantly improved classification of those classes.

4. Wavelet transformation

An image may be considered as a 2D signal of grey-level intensities. Transformations can be applied on images for signal processing in order to enhance image features. Wavelet functions represent a signal of limited duration, which are used to decompose the input signal (image) by applying wavelet transformation. In contrast to sines and cosines used as basis functions for Fourier analysis, wavelets are finite and well localized in both time (or location) and frequency (Wickerhauser 1994). The continuous *wavelet transformation*

$$F^W(a,b) = |a|^{-(\frac{1}{2})} \int_{-\infty}^{\infty} f(x)\Psi\left(\frac{x-b}{a}\right) \mathrm{d}x$$
$$\text{with} \quad a, b \in R \quad a \neq 0 \tag{1}$$

is a convolution of the signal $f(x)$ with the scaled and shifted versions of the mother wavelet

$$\Psi_{a,b}(x) = \frac{1}{\sqrt{|a|}}\Psi\left(\frac{x-b}{a}\right). \tag{2}$$

Equation (1) describes the details of $f(x)$ at a position b and resolution a.

We used wavelet transformation for decomposing images into so-called detail images by bandpass filtering in a specific direction. The detail image, as illustrated in figure 4, contains directional information at a certain scale. Thus, wavelet transformation allows us to decompose images into a set of subimages at selected scales. This is known as multiscale representation of depth d of the image I (Van de Wouver *et al* 1999). We performed a single level image decomposition for $d = 1$ using the Coiflet 2 and Pseudocoiflet 4 mother wavelets shown in figure 4. Within the detail images, Haralick texture features and their statistical moments were computed in the same way for the original FMS images. The reapplication of texture analysis within these detail images yields a variety of new texture features. Besides Haralick features in the transformed images, the band energy and histogram signature of the wavelet detail coefficients are additional texture features which are also used for classification. The wavelet histogram signature is characterized by its variance (α) and the decreasing rate of the histogram peak (β) (Van De Wouver 1998).

5. Classification

For classification we use the supervised classification method. This means texture facies are calibrated within homogenous sections called training intervals where core data are available (Benaouda *et al* 1999, Bartetzko *et al* 2002). From these training intervals, only 1000 randomly selected data points are used as samples for each texture class. We tested how many sampling points would be needed for robust classification starting from 500 to 1000 data points. We found that repeated measurements for 1000 randomly selected sampling points yield a robust classification. The resulting bias in classification is less severe than the possible noise introduced by the image acquisition (see figures 7 and 9). For each sampling point, texture features are calculated and combined in a feature vector $\vec{x} = (x_1, x_2, \ldots, x_p)$ which is labelled with the corresponding rock class. Considering four statistical moments of the distribution of eight Haralick feature values in a small interval, each data point of the training set is represented by a 32-dimensional feature vector and creates a point in a 32-dimensional feature space. Wavelet-based features increase the dimension of the space additionally (up to 136 dimensions).

If the feature values form well-separated clusters for each group in the feature space and if these clusters represent the distribution of the features to be evaluated, a computer-based classification method can be applied to classify unknown data points by texture features. Our approach for classification can be roughly summarized in two steps (Jain *et al* 2000):

(i) The feature extraction mode finds the appropriate set of features for describing the input patterns. Hence, a reduced set of features is selected which discriminates the different clusters best.
(ii) The classification step uses the classifiers defined within training intervals to assign an unknown data point to the group closest to the cluster.

5.1. Feature reduction

If all features are used, some of them may be correlated with each other and bear no further information. Other features may be unable to discriminate between different rock classes. These features are redundant and useless and may reduce the accuracy and stability of the classification process (Duda *et al* 2001). Therefore, we first identify those texture features which discriminate best. To this end, features must be found which keep the group clusters as compact as possible and at a maximum distance to each other. A common technique to achieve this is the *stepwise discriminant analysis* (Einslein 1977, Huang *et al* 2003).

This method analyses a ratio called *Wilks*'-Λ:

$$\Lambda(p) = \frac{\det(S_W(\vec{x}))}{\det(S_T(\vec{x}))}, \qquad \vec{x} = (x_1, x_2, \ldots, x_p) \tag{3}$$

where S_W is the *within-class scatter matrix*

$$S_W = \sum_{g=1}^{q} \sum_{i=1}^{n_g} (\vec{x}_{ig} - \vec{\mu}_g)(\vec{x}_{ig} - \vec{\mu}_g)^T. \tag{4}$$

This matrix is the sum of the *covariance matrices* for each of the q classes. The *covariance matrix* describes the scatter of the training vectors $\vec{x}_{ig}$ about the mean $\vec{\mu}_g$ of the gth group.

The second matrix in equation (3) is the *total-scatter matrix*

$$S_T = \sum_{i=1}^{n} (\vec{x}_i - \vec{\mu})(\vec{x}_i - \vec{\mu})^T \tag{5}$$

where $\vec{x}_i$ is a training sample and $\vec{\mu}$ the mean of all samples. Equation (5) describes the scatter of all features about a common mean. In both equations (4) and (5), the variable T stands for the transposed matrix.

To find the relevant features for classification, the stepwise procedure adds a feature (a further dimension) and the *partial* Λ*-statistics*,

$$\Delta\Lambda(p+1) = \frac{\Lambda(p+1)}{\Lambda(p)}$$

$$\text{for} \quad \Lambda(p+1) \quad \vec{x} = (x_1, x_2, \ldots, x_p, x_{p+1}), \tag{6}$$

is considered. The corresponding *F-statistics* (Einslein 1977),

$$F = \frac{(n-p-q)}{(q-1)} \frac{1-\Delta\Lambda(p+1)}{\Delta\Lambda(p+1)}, \tag{7}$$

is used to test the significance of the change of equation (3) by adding a feature. In equation (7), n is the total number of data points, q is the number of classes and p are the features (dimensions) under consideration. Equation (7) is also called *F-to-enter*. A corresponding F-statistics for removing a feature is also defined (Einslein 1977):

$$F_{\text{remove}} = \frac{(n-p-q+1)}{(q-1)} (\Delta\Lambda(p-1) - 1). \tag{8}$$

Equation (8) is called *F-to-remove*.

The procedure starts with the full set of all features. The F-to-remove value is calculated for each feature and the feature with the lowest value below a significance level is removed. The matrices S_W(4) and S_T(5) are updated and the F-to-enter value is calculated for those features which are currently not in the feature set. The feature with the highest F-to-enter value above a significance level is assigned to the reduced feature set. This is repeated until no features can be added or removed.

5.2. Classification

To classify a feature vector $\vec{x}$, the *Bayes* decision rule is used (Duda *et al* 2001):

$$b_g(\vec{x}) = -\tfrac{1}{2}\left(\vec{x} - \vec{\mu}_g^{\,T}\right)\Sigma_g^{-1}((\vec{x} - \vec{\mu}_g) + \log(\det(\Sigma_g)) \tag{9}$$

where Σ_g is the *covariance matrix* of the training samples of the gth class.

The feature vector $\vec{x}$ is assigned to that class with the largest *Bayes* value b_g.

The *Bayes* decision rule in equation (9) can be simplified (Einslein 1977) by the assumption that the *covariance matrices* Σ_g for all groups are identical and could be described by the mean of all *covariance matrices*:

$$\Sigma_g \approx \Sigma = \frac{1}{n-q} S_W. \tag{10}$$

Then the *Bayes* decision rule (equation (9)) becomes

$$b_g(\vec{x}) = \left(\vec{x} - \tfrac{1}{2}\vec{\mu}_g\right)\Sigma^{-1}\vec{\mu}_g^{\,T} + \text{const.} \tag{11}$$

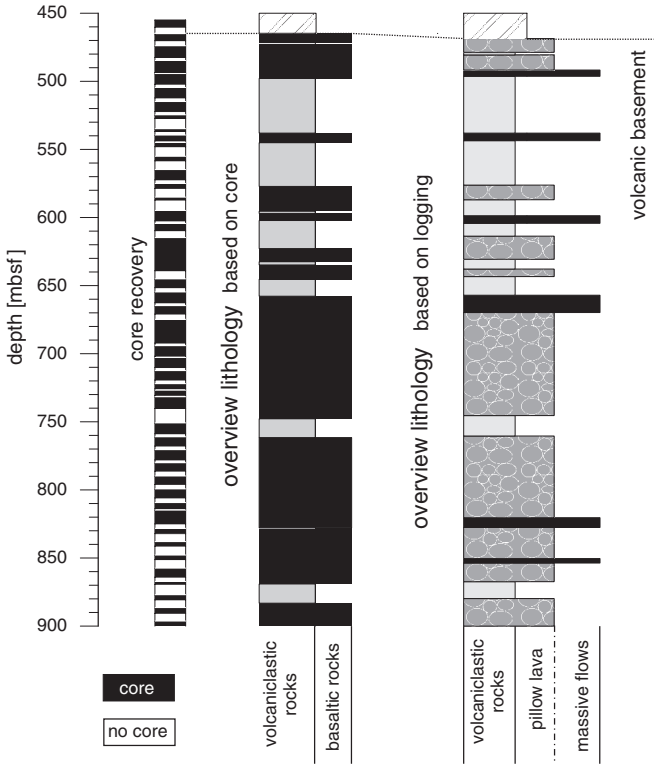

Figure 5. Lithology profile of ODP hole 1203A drilled at Detroit Seamount, Northwest Pacific Ocean during Leg 197 (in 2001). Core recovery and lithology based on core data and logging data are plotted versus depth in metres below seafloor (mbsf). Distinction between logging units is based on natural gamma ray, neutron porosity, bulk density and resistivity measurements (after Shipboard Scientific Party (2002)).

6. Application to ODP hole 1203A

We use FMS images from ODP hole 1203A which was drilled at Detroit Seamount (northwest Pacific Ocean) during ODP leg 197 (July–August 2001) (Shipboard Scientific Party 2002). Here, the volcanic basement was encountered at 457 m below seafloor (mbsf). The borehole recovered pillow lava, massive cores interpreted as basaltic lava flows, and volcaniclastic intercalations. Core recovery in hole 1203A was low (56.6%). Overview lithology profiles based on core and logging data are shown in figure 5. Standard logging operations included two runs of the FMS tool string. For reconstructing the volcanic basement, we focus on the first pass, which recorded FMS data in the basement section from 915 mbsf to 420 mbsf (Shipboard Scientific Party 2002).

6.1. Choice of texture facies

The following lithotypes could be distinguished from the logging data: pillow lava, partly fractured massive rocks and volcaniclastic rocks. Core data allowed distinction of volcaniclastic units, which are composed of tephra deposits (identified as basalt/lapilli tuff and breccia) and their resedimented derivatives, as well as clastic sediments made up of horizontally bedded siltstones, sandstones and mudstone (Shipboard Scientific Party 2002). If lithologies have the same log response (volcaniclastic sediments) but show different patterns in the FMS image, texture logs will be of great importance in reconstructing lithology. We assigned three texture classes for igneous rocks according to dynamically and statically normalized FMS images, core and logging data (see figure 6):

Massive rocks are highly resistive and homogenous units interrupted by conductive features continuing mostly horizontally over all four pads. These features are interpreted as fractures and veins cutting the borehole (training intervals: 535–539 mbsf).

Pillow lava is characterized by bright rounded regions, which are uniformly resistive with irregular fracture patterns. Pillow units are bounded by darker, more conductive intervals representing the altered hyaloclastic rim and interpillow zones (training interval: 465–491 mbsf).

Vesicular units are characterized by high resistivity with only a few conductive patches of variable size. Core description of vesicular basalts mentions that vesicles are partly filled with carbonate making them resistive and do not show a clear resistivity contrast to basaltic matrix. The classification of vesicles is limited to conductive fillings (training intervals: 888–890 mbsf).

and three classes for volcaniclastic textures:

Breccia has a dark, mottled FMS appearance with bright patches reflecting resistive clasts as well as brown patches corresponding to highly conductive components within a conductive matrix (training interval: 611–614 mbsf).

Layered sections are characterized by almost horizontal bedding structures: highly homogenous within a layer, but with clear contrasts across boundaries (training interval: 567–570 mbsf).

Resedimented rock refers to tuff and has chaotic (resedimented) patterns with a brownish background colour due to alteration. It may also consist of unaltered basaltic glass particles, which show up as tiny resistive patches (training interval: 503–507 mbsf).

Note that 1000 sampling points are randomly selected within these training intervals. All four pads are used for sample selection. Hence, the minimum length of a training interval is 62.5 cm for this number of sampling points (minimum of 250 sampling points per pad = 1000 sampling points for the sampling rate of 2.5 mm of the logging tool). We have chosen larger training intervals due to internal variation in rock texture. Random selection in these larger intervals and its correct classification proved the robustness of this classification in reliability checks prior to classification.

6.2. Results from Haralick texture features

Discriminant analysis was used first to check the calibration reliability. Since training for each run was performed at 1000 randomly picked sample points, we did not use the entire intervals for training. Hence, the entire training intervals were

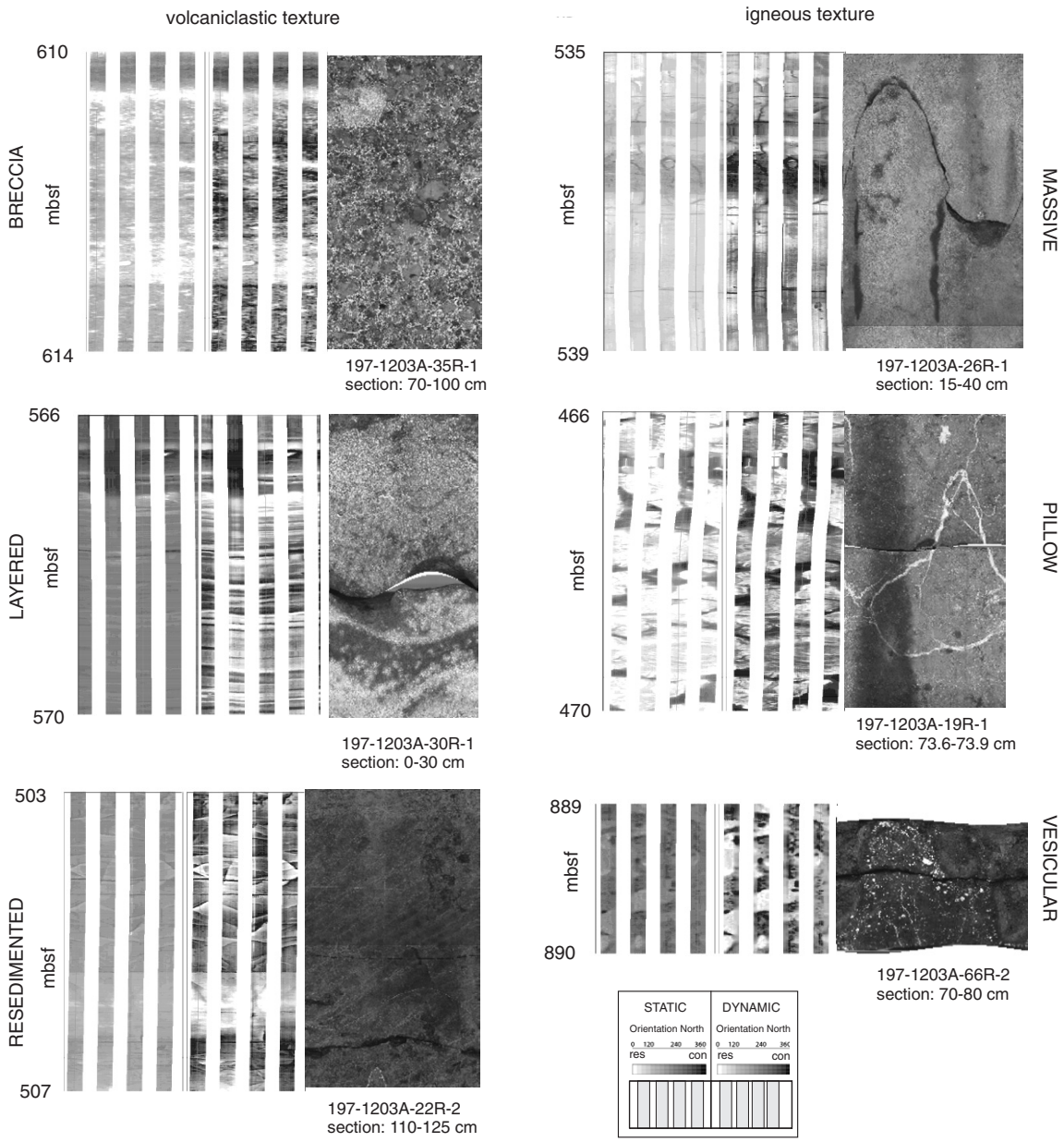

Figure 6. FMS texture facies assigned in ODP hole 1203A drilled at Detroit Seamount, Northwest Pacific in 2001. Core scan images give a detailed view of the corresponding depth interval.

used for a first classification check after each run. Sampling picking and training was performed in ten distinct runs in order to check the reproducibility of classification. The result is shown in figure 7. The best run out of these ten performances was chosen to classify the entire FMS set. Stepwise linear discriminant analysis used all texture features.

In total, 89.9% of the depth points were correctly classified into the same texture facies as in the calibration training class by weighting the correct classification percentage with sampling points. The percentage of consistent classification is above 90% for the breccia class, the fractured class and pillow class, but is lower for the layered as well as the resedimented class (>80%), and below 75% for the vesicular class. However, these percentages indicate that the texture facies can be recognized by discriminant analysis. This is a necessary condition for classifying the remaining intervals of Hole 1203A.

The final result of the synthetic lithology profile is called the texture log and is displayed in figure 8. Since the FMS sampling interval is 2.5 mm, the discriminant analysis might yield unreasonable layers of this thickness—represented only by one depth point. We chose a 1 m depth interval, where the dominant class within this interval defines the classification. Therefore, our texture profile has a resolution of 1 m. As mentioned above, the borehole caliper mainly controls the image quality. Hence, caliper data are used to avoid misclassifications due to washouts. If the caliper exceeds 15 in, classification data are discarded from the texture log. The classification was also neglected if either all four pads or both pad pairs yielded different results (distinctive classification).

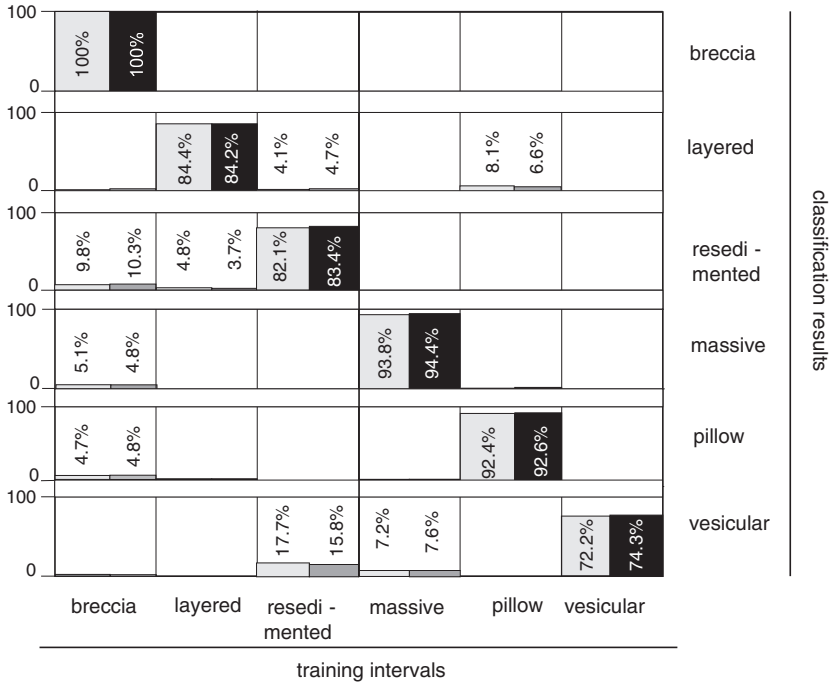

Figure 7. Performance matrix obtained from Haralick training. Grey shaded bar charts represent the average classification derived from 10 Haralick runs. The black and diagonal bar charts represent the right classification for each class achieved in the selected Haralick run, whereas the other black bar charts display the misclassification obtained by the chosen run.

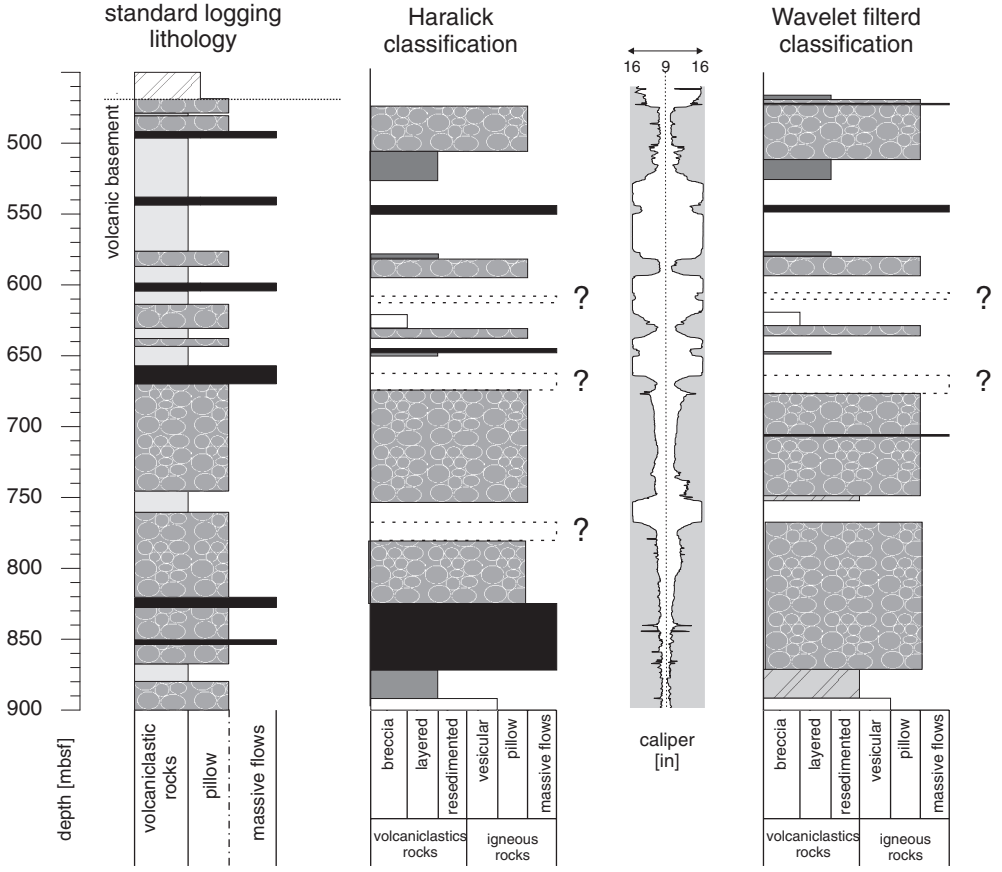

Figure 8. Standard logging lithology (left-hand side) and results from discriminant analysis based on calculation of rotation invariant Haralick features (middle) as well as results from the combination of Haralick features and wavelet transformation (right-hand side).

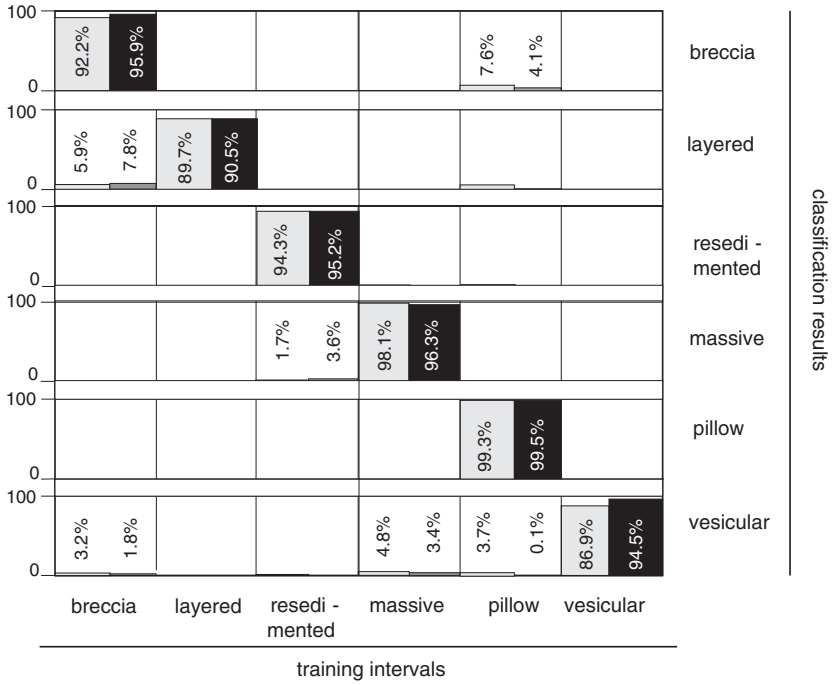

Figure 9. Performance matrix obtained from the combination of Haralick and wavelet training. Average classification data derived from five tests are displayed in grey shaded bar charts, whereas the black bar charts represent the classification obtained from the selected run.

Figure 8 illustrates that the quality of classification is mainly controlled by caliper data. Most of the classification gaps are caused by borehole enlargements. Only three zones (at 600 mbsf, 650–658 mbsf, 760–768 mbsf) could not be clearly classified. Their results were discarded from the profile.

Overall, the texture profile and the logging facies agree well. In particular, pillow texture units consistently occur in both texture and logging profiles. The occurrence of volcaniclastic classes, separated into three distinctive texture groups, corresponds well to the core and logging data shown in figure 5. Layered and vesicular classes only occur within their training intervals. The 1 m profile resolution avoids detection of smaller intercalations, which will be discussed later. However, there is one zone that significantly differs from the overview lithology. Within the texture profile, we classified the depth interval between 816 and 864 mbsf as massive rock. The logging profile defines this zone as a pillow-dominated section. Due to this mismatch, we applied filter functions on image data prior to texture analysis. Filtered image signals may yield a lower misclassification for problematic texture classes.

6.3. Filtering by wavelet transformation

Wavelet transformation was applied for filtering the FMS image signal. Here, we used a combination of wavelet functions (see section 4) to decompose the FMS signal. Extensive tests showed an improvement in classification when using a diagonal detail image derived from a Pseudocoiflet 4 wavelet combined with a vertical detail image based on a Coiflet 2 wavelet. Both filtered sub-images increased the feature space. Stepwise linear discriminant analysis removed ten features from the feature space including redundant classification information.

The performance matrix of the reliability check is displayed in figure 9. It shows higher classification consistency than the Haralick-based classification. In total, 98.0% of the depth points were correctly classified. This classification result reveals the percentage of all correctly classified sampling points out of all data points in all sampling intervals. The high number is mainly achieved by the almost 100% classification of the long pillow training interval. Except for breccia, all classes increased their level of correct classification. Due to the application of wavelet filtering, we particularly improved classification for the vesicular rock class, the most problematic class of the previous Haralick classification. On average 86.9% was correctly classified in contrast to the previous Haralick classification (only 72.2%; compare figures 9 and 7). For the run we applied on FMS images, we even correctly classified 94.9% of the training interval (black bars in figure 9), that is, a classification improvement of 18%. We also significantly increased correct classification for resedimented rock facies from 82.1% to 94.3%. Improved reliability checks increase confidence in the robustness of our discriminant analysis. The robustness was proven by five repeated measurements. Their average classification results are displayed as grey shaded bars in the performance matrix (see figure 9).

This new linear discriminant function was again applied to the first FMS run of ODP hole 1203A. The resulting profile is displayed in figure 8. It is seen that wavelet-based Haralick classification changed the massive classification to pillow classification. The reliability check shows that the classification of pillow and massive classes improved from Haralick-based classification to wavelet-filtered classification and is about 100%. It also shows that the gap below 750 mbsf

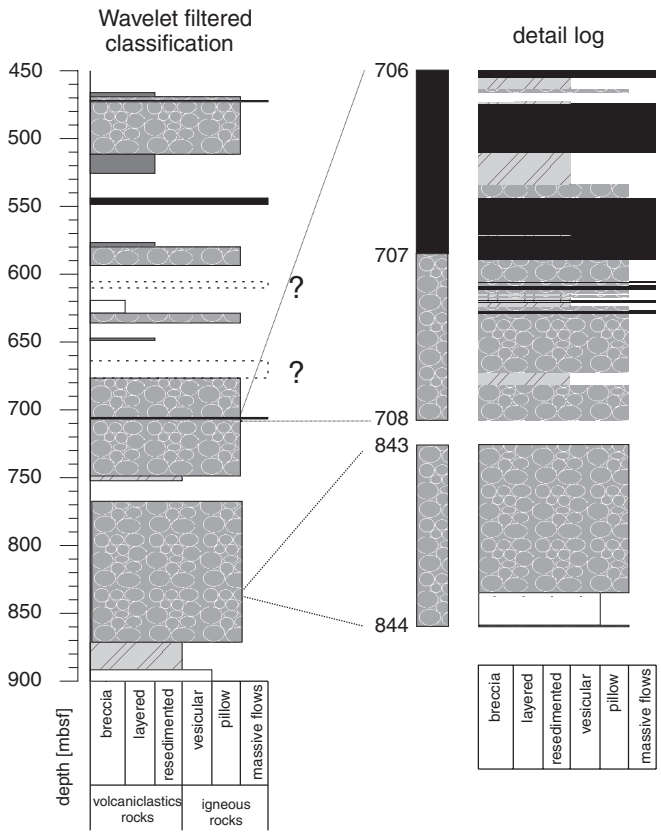

Figure 10. The left-hand side shows an overview of lithology derived from a 1 m resolution. The right-hand side shows the detailed texture log of two sections, where the resolution was set to 2.5 mm (tool sampling rate). It shows that dominant classes such as pillow and massive units are built up of interpillow material, vesicular zones and volcaniclastic intercalations.

from Haralick classification (see section 6.2) disappeared. The wavelet transformation improved the determination of layered and resedimented tuff classes too.

6.4. Quantification of rock classes derived from conventional logging, core recovery and FMS image data

Since we improved the total classification by application of wavelet filtering prior to Haralick feature generation, we discuss the quantification of the computed classes in more detail. The chosen resolution of 1 m is sufficient to obtain an overview lithology. However, the volcaniclastic rock classes may occur in layers thinner than 1 m or as filling material between pillows. To test this, we increase the resolution to improve the quantification of rock types especially for interpillow material and intercalations. Figure 10 shows two detailed sections representing classification results based on a 2.5 mm sampling rate. The dominant rock class of the 1 m intervals was taken for the overview lithology. The detailed classification reveals thinner intercalations of volcaniclastic material such as breccia, resedimented structures in massive- and pillow-dominated 1 m intervals as well as vesicular intercalations in pillow units.

The upper detail log between 706 and 707 mbsf may correspond to cores 197-1203A-45R-2, 197-1203A-45R-3 and 197-1203A-45R-4. The low core recovery of 56.6% (see above) makes it difficult to fit core and logging data exactly. These cores recovered in the depth interval between 704.6 and 708.8 mbsf are described as moderately olivine-phyric basalt with some glassy lobe margins. In the lobe interiors the core is fine grained and glassy lobe margins are replaced by dark green clay. There is brecciation of glassy lobe margins between lobes. The morphologies of the upper core (45R-2) suggest this core section is part of a subaerial pahoehoe flow (Shipboard Scientific Party 2002). These core observations agree with the detailed texture log in this depth interval. The upper section was predominately classified as massive flow, whereas the lower part was mainly classified as pillow. The brecciation and alteration of glassy lobe margins is expressed by tiny intercalations of the breccia and resedimented texture rock class. The core description and detailed texture profile agree well. The lower detail log between 843 and 844 mbsf shows a texture log section dominated by pillow classification with an intercalation of vesicular rocks. In corresponding cores 197-1203A-61R-3 and 62R-1 between 840.65 and 848.9 mbsf (poor recovery) rock structures are described as lobed. Fine-grained material is moderately to highly versicular with a patchy vesicle distribution (Shipboard Scientific Party 2002). This core description agrees with our texture classification.

The detailed texture log was confirmed by corresponding core description. What is then the result of an overall comparison of class quantities between conventional logging data, recovered cores and image texture analysis? The exact quantity of interpillow material and intercalations in oceanic lithosphere is still a subject of debate and therefore was derived based on the classification resolution of the sampling rate of 2.5 mm. Diagrams in figure 11 present quantitative estimates of diverse rock classes derived from the three sources of information: conventional logging data, core recovery and image texture logs.

Conventional logging data were roughly grouped into three classes by the Leg 197 ODP Logging Staff scientists. They provide continuous information with a sampling interval of 15 cm (6 inch) (Goldberg 1997) and allow distinction between volcaniclastics (34%), pillow units (57%) and massive rock classes (9%). The diagram derived from conventional logging data in figure 11 shows that pillows are the main rock type of this borehole. Core recovery was low (56.6%, see above). However, the quantity of volcaniclastic rocks (30%) derived from core data is close to that from logging data (see figure 11). The analysis of cores separated volcaniclastic rocks into breccia (5%), layered materials (13%) and resedimented rocks (12%). For igneous rocks a distinction is made between vesicular (27%), pillow (20%) and massive rock (23%) classes. Igneous rocks are more or less equally distributed based on core data. FMS image data record borehole wall resistivity with a sampling interval of 2.5 mm (0.1 inch) (Goldberg 1997) and provide continuous and high-resolution information. Images allowed a distinction between the following three volcaniclastic units to be made: breccia (13%), layered (6%) and resedimented (16%). In total, 35% of the data are classified into volcaniclastic units

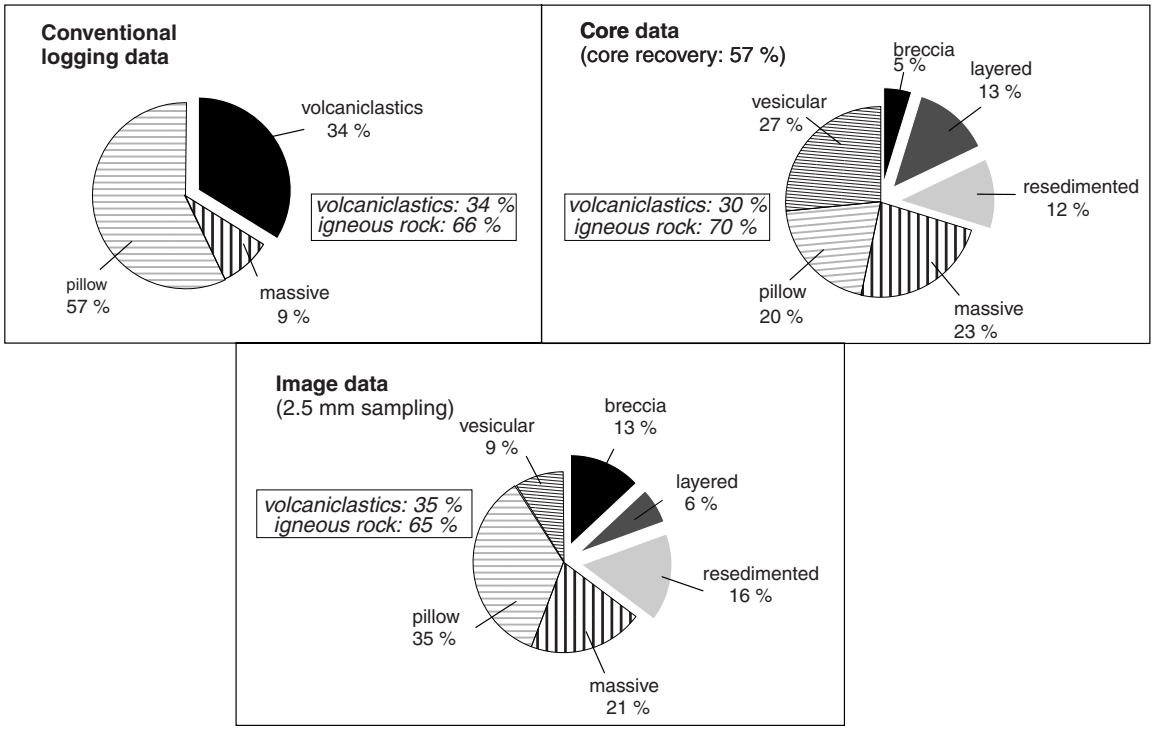

Figure 11. Pie charts derived from conventional logging data, core data and image texture analysis, representing the quantity of rock classes recovered in ODP hole 1203A.

(see figure 11), in excellent agreement with logging data analysis (30%), but with the additional advantage of yielding more detailed information on the variety of volcaniclastic rocks. Igneous rocks covered 65% of the texture classification. In detail, 21% was assigned to massive units, 35% to pillows and 9% to vesicular units. Here, the pillow is also the dominant rock class of the texture classification. There are slight differences between conventional log and image texture classification. First, conventional logging data have been roughly summarized by the ODP Logging Staff scientist and show a different resolution and the fewest groups. It represents more or less a rough estimate of class quantities. Core data estimates present slightly different amounts of breccia, layered units, pillows and vesicular rocks. The question arises now whether this estimate is reliable since it is only based on poor core recovery. It could be that vesicular rocks recovered in this hole would have been classified as pillows if their hyaloclastic rim was recovered as well. However, for the most important information, the quantity of volcaniclastic material and igneous rocks, there is excellent agreement between all methods applied to ODP hole 1203A.

7. Summary and conclusions

We successfully performed the transformation of images in quantitative log curves applying pattern recognition analysis. Hence, this transformation allows us to perform an objective classification of FMS borehole wall images acquired in ODP hole 1203A. We applied texture analysis to study second-order image parameters defined as Haralick features. Within training intervals, we defined texture classes for igneous rocks as massive rocks, pillows and vesicular units; volcaniclastic rocks were classified as breccia, layered rocks and resedimented units. Stepwise linear discriminant analysis was used to distinguish between rock classes based on computed texture features. The Bayesian decision rule was applied to classify borehole wall images. Caliper data acquired with the FMS tool are used for quality control: if the diameter exceeds 15 inches and no dominant pad classification could be obtained, classification results are discarded from the texture profile. Results based on Haralick texture features agree well with the lithology derived from standard logging data. Below 800 mbsf, logging and texture profiles disagree strongly. Image filtering was implemented by a single-level decomposition applying wavelet transformation. Here, detailed images obtained by the Pseudocoiflet 4 (diagonal) and the Coiflet 2 wavelets (vertical) enhance the directional image information. Then texture analysis was applied yielding an improved classification for the defined rock classes. A synthetic profile resulting from a combination of wavelet-transformed images agrees well with the logging-based profile. Comparison of rock classes between conventional logging data, recovered core data and image texture data reveals an excellent agreement with respect to the estimated quantity of volcaniclastic material and igneous rocks. Application of pattern recognition analysis allows us to transform image patterns into signals. Application of pattern recognition techniques permits an objective analysis of digital borehole wall images. Texture analysis allows us to classify image data based on statistics of the digital image data. It offers the potential to facilitate objective analysis of multiple boreholes with the same lithology.

Acknowledgments

This project was funded by the German Science Foundation DFG by operating grant CL 121/19-1 to C Clauser, T Berlage and R Pechnig. We used data provided by the Ocean Drilling Program (ODP). The ODP was sponsored by the US National Science Foundation (NSF) and participating countries under management of the Joint Oceanographic Institutions (JOI), Inc. We gratefully acknowledge advice from Anne Bartetzko (Bremen University) and Volker Rath (RWTH Aachen University) as well as the support provided by Peter Wisskirchen (FIT Fraunhofer Institute).

References

Barr S, Revillon S, Brewer T, Harvey P and Tarney J 2002 Determining the inputs to the Mariana subduction factory: using core-log integretation to reconstruct basement lithology at ODP hole 801C *Geochem. Geophys. Geosyst.* **3** 1–26

Bartetzko A, Paulick H, Iturrino G and Arnold J 2003 Facies reconstruction of a hydrothermally altered dacite extrusive sequence: evidence from geophysical downhole logging data (ODP Leg 193) *Geochem. Geophys. Geosyst.* **4** 1–24

Bartetzko A, Pechnig R and Wohlenberg J 2002 Interpretation of well-logging data to study lateral variations in young oceanic crust: DSDP/ODP holes 504B and 896A, Costa Rica Rift *Geological Applications of Well Logs: AAPG Methods in Exploration* vol 13 ed M Lovell and N Parkinson (Tulsa, OK: American Association of Petroleum Geologists) pp 213–28

Benaouda D, Wadge G, Whitmarsh R B, Rothwell R and MacLeod C 1999 Inferring the lithology of borehole rocks by applying neural network classifiers to downhole logs: an example from the ocean drilling program *Geophys. J. Int.* **136** 477–91

Cheung P S 1999 Microresistivity and ultrasonic imagers: tool operations and processing principles with reference to commonly encountered image artefacts *Borehole Imaging: Application and Case Histories* (*Special Publications* vol 159) ed M A Lovell, G Williamson and P K Harvey (London: Geological Society) pp 45–57

Cooper P, Arnaud H M and Flood P G 1995 Formation MicroScanner logging responses to lithology in guyot carbonate platforms and their implications: sites 865 and 866 *Proc. Ocean Drill. Program Sci. Results* **143** 329–72

Delhomme J P 1992 A quantitative characterization of formation heterogeneities based on borehole image analysis *33rd Ann. Logging Symp. Soc. Professional Well Logging Analysts (SPLWA) (14–17 June 1992)*

Duda R O, Hart P E and Stork D G 2001 *Pattern Classification* 2nd edn (New York: Wiley)

Einslein K 1977 *Statistical Methods for Digital Computers* vol 3 (New York: Wiley)

Goldberg D 1997 The role of downhole measurements in marine geology and geophysics *Rev. Geophys.* **35** 315–42

Harris D A, Lewis J J M and Wallace D J 1993 The identification of lithofacies types in geological imagery using neural networks *Proc. European Conf. on Artificial Intelligence in Petroleum Exploration and Production (EUROPCAIPEP) (20–22 September 1993)* vol 93 pp 1–9

Huang K, Velliste M and Murphy R 2003 Feature reduction for improved recognition of subcellular location patterns in fluorescence microscope images *Proc. Int. Society Opt. Eng. (SPIE)* **4962** 307–18

Jain A K, Duin R P W and Mao J 2000 Statistical pattern recognition: a review *IEEE Trans. Pattern Anal. Mach. Intell.* **22** 4–37

Knecht L, Mathis B, Leduc J-P, Vandenabeele T and Di Cuia R 2003 Electrofacies and permeability modelling in carbonate reservoirs using image texture analysis and clustering tool *44th Ann. Logging Symp. Soc. Professional Well Logging Analysts (SPLWA) (22–25 June 2003)*

Lovell M A, Harvey P K, Brewer T S, Williams C, Jackson P D and Williamson G 1998 Application of FMS images in the Ocean Drilling Program: an overview *Geological Evolution of Ocean Basins: Results from the Ocean Drilling Program (Special Publications* vol 131*)* ed A Cramp, C J MacLeod, S V Lee and E J W Jones (London: Geological Society) pp 287–303

Luthi S M 1994 Textural segmentation of digital rock images into bedding units using texture energy and cluster labels *Math. Geol.* **26** 181–96

Machecler I and Nadal J-P 2004 Pre-attentive segmentation of oriented textures *J. Geophys. Eng.* **1** 312–26

Pechnig R, Haverkamp S, Wohlenberg J, Zimmermann G and Burckhardt H 1997 Integrated log interpretation in the German continental deep drilling program: lithology, porosity, and fracture zones *J. Geophys. Res.* **102** 18363–90

Pezard P, Lovell M and Hiscott R 1992 Downhole electrical images in volcaniclastic sequences of the Izu-Bonin forearc basin, western Pacific *Proc. Ocean Drill. Program Sci. Results* **126** 603–23

Serra O 1986 *Fundamentals of Well-log Interpretation: 2. The Interpretation of Logging Data* (New York: Elsevier)

Shipboard Scientific Party 2002 Leg 197: motion of the Hawaiian Hotspot: a paleomagnetic test *Proc. Ocean Drill. Program Initial Rep.* **197**

Tilke P G, Allen D and Gyllensten A 2006 Quantitative analysis of porosity heterogeneity: application of geostatistics to borehole images *Math. Geol.* DOI: 10.1007/s11004-005-9011-y

Tuceryan M and Jain A K 1998 Texture analysis *The Handbook of Pattern Recognition and Computer Vision* ed C H Chen, L Pau and P Wang (New York: World Scientific) chapter 2.1, pp 207–48

Tyagi A K and Bhaduri A 2002 Porosity analysis using borehole electrical images in carbonate reservoirs *43rd Ann. Logging Symp. Soc. Professional Well Logging Analysts (SPLWA) (2–5 June 2002)*

Van De Wouver G 1998 Wavelets for multiscale *PhD Thesis* University of Antwerp

Van de Wouver G, Scheunders P and Van Dyck D 1999 Statistical texture characterization from discrete wavelet representations *IEEE Trans. Image Process.* **8** 592–8

Wickerhauser M V 1994 *Adapted Wavelet Analysis from Theory to Software* (Wellesley, MA: A K Peters)

Ye S, Rabiller P and Keskes N 1998 Automatic high resolution texture analysis on borehole imagery *39th Ann. Logging Symp. Soc. Professional Well Logging Analysts (SPLWA) (26–29 May 1998)*